Structure, Location and Spatial Proximities of Hydroxyls on γ-alumina Crystallites by High-Resolution Solid-State NMR and DFT Modeling: Why Edges hold the Key

Ana Teresa Fialho-Batista, Thomas Pigeon, Jordan Meyet, Dorothea Wisser, Mickael Rivallan, David Gajan, Leonor Catita, Fabrice Diehl, Anne-Sophie Gay, Céline Chizallet, et al.

Structure, Location and Spatial Proximities of Hydroxyls on γ–Alumina Crystallites by High-Resolution Solid-State NMR and DFT Modeling: Why Edges hold the Key

Ana T. F. Batista [a,$], Thomas Pigeon [a,$], Jordan Meyet [a], Dorothea Wisser [a,b,+], Mickael Rivallan[a], David Gajan[b], Leonor Catita[a], Fabrice Diehl[a], Anne-Sophie Gay [a], Céline Chizallet [a], Anne Lesage [b,*], and Pascal Raybaud [a,c,*]

[a] IFP Energies nouvelles, Rond-point de l'échangeur de Solaize, 69360 Solaize (France)

[b] Université de Lyon, CNRS, ENS Lyon, Université Lyon 1, Centre de RMN à hauts champs de Lyon, UMR 5082, 5 rue de la Doua, 69100 Villeurbanne (France)

[c] ENS Lyon, CNRS, Laboratoire de Chimie UMR 5182, 46 Allée d'Italie, 69364 Lyon (France)

[$] A.T.F.B and TP contributed equally to this paper.

[+] current address: Erlangen Center for Interface Research and Catalysis, Friedrich-Alexander-Universität Erlangen-Nürnberg, Egerlandstrasse 3, 91058 Erlangen (Germany)

ABSTRACT

The atomic-scale characterization of surface active sites on γ–alumina still represents a great challenge for numerous catalytic applications. Here, we combine advanced DFT calculations with one- and two-dimensional proton solid-state NMR experiments to identify the exact location and the spatial proximity of hydroxyl groups on γ–alumina crystallites. Our approach relies on revisited models for the (100), (111), basal $(110)_b$ and lateral $(110)_l$ facets, as well as for the edges at their intersections. Notably, we show that the ≃0 ppm Al_{Td}-μ_1-OH protons are predominantly located on edges, where these are free from the H-bond network. The proximities among the Al_{Td}-μ_1-OH as well as with μ_2-OH groups are revealed by ^{1}H-^{1}H dipolar correlation experiments and analyzed in the light of the DFT calculations, which identify their location on the basal $(110)_b$ facet, and on the $(110)_b$/(100) and $(110)_b$/$(110)_l$ edges. Using chlorine atoms to probe the presence of hydroxyls, we show that the chlorination occurs selectively by exchanging μ_1-OH located on edges and on lateral $(110)_l$ facets. By contrast, the basal $(110)_b$ and lateral (111) facets are not probed by Cl. This exchange explains the disappearance of the ≃0 ppm peak and of the correlations involving Al_{Td}-μ_1-OH species. Moreover, after chlorination, a deshielding of the Al_{Td} is observed on high-resolution ^{27}Al NMR spectra. More subtle effects are visible on the proton correlation spectra, which are attributed to the disruption of the H-bond network in the course of chlorination.

KEYWORDS: gamma-alumina, nuclear magnetic resonance, density functional theory, hydroxyl, edge, chlorine

I. Introduction

Aluminas are highly valued materials for their versatility in various catalytic processes such as biomass conversion,[1,2] olefin metathesis,[3,4] natural gas conversion,[5] petrochemistry[5,6] and exhaust gas cleaning,[7,8] as a result of their tuneable surface physico-chemical properties.[6] Gamma-alumina (γ–Al_2O_3) is one of the most widely used alumina polymorphs.[9,10] Since the early work of Knözinger and Ratnasamy,[11] the nature and atomic-scale structure of surface hydroxyl (-OH) groups on γ–Al_2O_3 surface have been thoroughly examined using various spectroscopic[12-25] and computational approaches.[18,20,26-32] This extensive search for an ever more refined determination of the γ–Al_2O_3 surface chemistry is motivated by the need to better control, on the one hand, the intrinsic reactivity driven by the Brønsted and Lewis surface sites for various reactions,[33,34] and on the other hand, the grafting, the impregnation and the activation of metal precursors on γ–Al_2O_3 acting as a catalytic support.[4,10,35] However, the surface structural features of γ–Al_2O_3 are still questioned due to its complexity at multiple scales, from crystallite morphology to crystallinity or hydration level. As a result, the detailed distribution, location and molecular structure of the reactive aluminum and hydroxyl sites remain questioned.[36]

Over the years, solid-state nuclear magnetic resonance (NMR) spectroscopy[14-16,19-22,24,37] often in combination with other analytical approaches such as infra-red (IR) spectroscopy[11-13,16-18,23] has emerged as a method of choice to characterize the surface structure of γ–Al_2O_3. One-dimensional (1D) ^{1}H NMR spectroscopy provides distinct resonances for the various hydroxyl groups with key structural features. The information content has been further increased by two-dimensional (2D) proton-proton spectroscopy or by heteronuclear correlation experiments with other NMR-active probe nuclei such as ^{27}Al[21,24] or ^{17}O.[22,37] In parallel, the adsorption of probe molecules provided additional spectroscopic signatures, helping to discern the various surface sites.[38] The use of high-

and ultra-high magnetic fields that drastically improve spectral resolution has recently opened up new opportunities for the characterization of the surface hydroxyl groups by NMR. New environments for five-coordinated Al sites were described at 35.2 T.[24] The coordination of O atoms involved in OH groups as well their non-random spatial proximities were also unambiguously identified at high magnetic field.[22] More recently, 2D correlation experiments carried out at 18.8 T allowed the identification of spatial proximities between the various hydroxyl groups: μ_n-Al_x-OH with n=1 to 3 and x=IV (tetracoordinated), V (penta-coordinated), VI (hexacoordinated), leading to a detailed description of the hydroxyl network structure.[39]

Density functional theory (DFT) simulations were also employed to provide more relevant bulk[40] and surface[26-29] models with hydration states controlled by temperature and water pressure, which can be used jointly with experimental data to get insight into the structure of acid sites. DFT calculations of the ^{27}Al and ^{1}H chemical shifts[19,41,42] were notably employed to revisit some earlier empirical assignments, providing a rational bridge between experimental observations and μ_n-Al_x-OH architecture. An unambiguous assignment of the various NMR signals to specific hydroxyl sites from DFT calculations remains however challenging as the H-bond network strongly perturbs the proton chemical shifts. Recent DFT calculations reported by Batista et al.[42] revealed that the proton resonance at a $\simeq$3 ppm chemical shift conventionally assigned to μ_3-Al_x-OH groups[19] predominantly corresponds to H-bond donor μ_n-Al_x-OH groups (including n=1 or 2) present on the alumina (110) and (111) facets, and which were neglected beforehand. This revised interpretation was proposed in the light of DFT calculations considering a novel atomistic edge model located at the intersection of the (110) and (100) facets.[42] These models suggest that the upfield signal at $\simeq$0 ppm should be assigned to "free", non H-bond donor, μ_1-Al_{Td}-OH present on the edges of the crystallites, in the spirit of an empirical proposal made by Busca.[13] In the NMR-

DFT study,[42] chlorine was shown to be a rather simple but relevant probe atom selectively exchanging μ_1-Al_x-OH groups.[18,42] More recently, ^{1}H-^{1}H 2D experiments pinpoint the potential existence of two distinct μ_1-Al_{Td}-OH sites presumably located at the edges of needle shaped γ–Al_2O_3 particles.[43]

These findings highlighted the importance of going beyond standard alumina facets, as well as the need of increasingly accurate facet and edge models, as exhaustive as possible, so as to provide a reliable interpretation of spectroscopic experiments. They also underlined the need for a more refined determination of spatial proximities among the various families of hydroxyls at the γ–alumina surface. Striving towards this ideal, the determination of more representative γ-Al_2O_3 facet models was recently proposed[44] from the simulation of the topotactic transformation of the boehmite (γ–AlOOH) precursor under thermal treatment as expected from usual experimental synthesis pathways.[9] With this approach, the finite nature of the boehmite crystallites was considered to revisit relevant γ-Al_2O_3 facet models inherited by parentage to the γ–AlOOH facets.[44-46] However, the way these new facet models impact our view at the atomic scale of the edges has not been explored so far.

Herein, using these revisited slab models as well as novel alumina edge models, we further refine our understanding of the location, structure and local environment of γ-Al_2O_3 surface hydroxyl groups, using chlorine as a selective probe. One-dimensional ^{1}H and ^{27}Al spectra, as well as two-dimensional ^{1}H-^{1}H and ^{1}H-^{27}Al correlation experiments recorded at high magnetic fields on plain and chlorinated γ-alumina samples are interpreted in the light of these calculations. Thanks to this combination of experiments and calculations, we provide a revisited assignment of the main features of the 1D and 2D proton NMR spectra of γ-Al_2O_3, to an extent which was not possible

from previous simplified facet models. We also analyse and compute the behaviour of chlorine on facets and edges, to get a finer knowledge on the local arrangements of hydroxyl groups. These findings first validate the revisited facet and edge models proposed and second, provide an unequalled level of knowledge on the distribution of OH groups at alumina surfaces, which is expected to orient future work on the link between morphology and reactivity of alumina crystallites.

II. Methods

II.1 Alumina samples

The studied γ–alumina sample (called P-egg in our previous work[42]) is obtained from commercial boehmite powder from Sasol PuralSB3. As recalled in **supporting information SI 1**, it exhibits a BET surface measured by N_2 physisorption of 183 $m^2\ g^{-1}$. HR-TEM revealed that it is composed of rounded crystallites (with average dimensions of 12.5 x 6 x 5 nm) presenting (110) and (100) facets such as investigated in the DFT simulations.[42]

Chlorinated alumina samples were prepared by exposing alumina to a HCl solution ($3.5\%_{w}Cl/g_{dry\ alumina}$) for 45 minutes, followed by drying and calcination at 793 K. The two chlorine loadings of γ–alumina investigated here are 0.5 wt % and 1.4 wt %Cl which correspond to approximately 0.5 Cl nm^{-2} and 1.4 Cl nm^{-2}.

Chlorinated and non-chlorinated samples thermally treated under H_2 for 2h at 500°C (ramp 5°C/min) and conditioned under vacuum were analyzed by 1D and 2D ^{1}H NMR. 1D ^{27}Al and 2D $^{1}H\{^{27}Al\}$ NMR experiments were used to analyze the non-chlorinated alumina sample dehydroxylated at 450 °C in vacuo.

II.2 NMR experiments

All ^{1}H and ^{27}Al solid-state NMR spectra were obtained on a Bruker Avance III 18.8 T spectrometer (800 MHz ^{1}H Larmor frequency and 208.5 MHz ^{27}Al Larmor frequency) using zirconia 2.5 mm rotors at a magic angle spinning (MAS) frequency of 30 kHz. The proton and aluminum spectra were externally referenced to respectively the proton peak of adamantane to 1.87 ppm and to a static 1M solution of aluminum nitrate (0 ppm). Quantitative ^{1}H spectra were recorded using a DEPTH sequence for probe background suppression.[47-49] For these experiments, pre-scan delays were set to five times the ^{1}H longitudinal relaxation time (T_1). The 2D proton single quantum (SQ) double quantum (DQ) correlation spectra were recorded according to the following general scheme: excitation of DQ coherences, t_1 evolution and reconversion into observable magnetization, Z-filter, and detection. DQ excitation and reconversion were achieved using the BABA pulse sequence (two rotor periods of the BABA recoupling sequence for excitation and reconversion of DQ coherences).[50] Proton $\pi/2$ pulses were set to 2.5 μs in all experiments. Proton decoupling was always carried out using SPINAL-64 at a radio frequency field of 100 kHz.[51] The two-dimensional ^{1}H-^{27}Al experiment was recorded using a proton-detected dipolar-based HMQC pulse sequence,[52] with the $SR4_1^2$ recoupling scheme.[53] Quadrature detection in ω_1 was achieved using the States-TPPI method for all 2D experiments.[54] Single pulse ^{27}Al spectra were recorded using a single-pulse experiment (1024 scans) with a high power SPINAL-64 proton decoupling during acquisition (100 kHz).

II.3 DFT Modeling

A plane-wave basis set with a 400 eV energy cutoff was used in conjunction with the projector augmented wave (PAW) method for the pseudo potentials as implemented in the Vienna Ab-initio Simulation Package (VASP).[55,56] The exchange correlation functional used was the one proposed by Perdew, Burke and Ernzerhof (PBE)[57] with density dependent dispersion correction according to dDsC formalism.[58,59] The energy of the reference water molecule has been computed at the same level of approximation in a cubic box of 10 Å at the gamma point. A Gaussian smearing was used with a width of 0.05 eV and the convergence criterion for the SCF cycles was set at 10^{-7} eV. The convergence criterion for geometric relaxation was set to 0.01 eV $Å^{-1}$ on each atom of the slab and nano-rod models used to describe facets and edges.

DFT calculations were thus performed on three main hydroxylated γ-Al_2O_3 facets, namely the lateral $(110)_l$ and (111) facets and the basal $(110)_b$ facet as determined by Pigeon et al.[44] In the conditions representative of pretreatment of the samples before NMR acquisition, the (100) surface is dehydroxylated. We considered 4 relevant facet structures representing the $(110)_l$ facet: $(110)_l$-A1, $(110)_l$-A2, $(110)_l$-L1, $(110)_l$-L2, and 3 distinct ones for the (111) facet: (111)-D1, (111)-D2 and (111)-P1_2. All details on the construction of these models and the different types of hydroxyls present depending on the temperature and water pressure conditions can be found in ref.44 and the corresponding molecular structures of the simulated facets are accessible from the Nomad repository.[60]

To simulate edge structures, we have used a similar method based on nano-rod models as explained in ref.42 All technical aspects are provided in **supporting information SI 2**. Three new edge models, namely the $(110)_b$/(100), $(110)_b$/$(110)_l$-A1, $(110)_b$/$(110)_l$-L1 were constructed, in addition to the previous (100)/$(110)_l$-A1 one established in ref.42. In particular, two types of $(110)_b$/$(110)_l$

rods were built as to take into account the nature of the two major types of $(110)_l$ facets, labelled L1 and A1 according to ref.44.

Various hydroxyl coverages of facets and edges have been explored. However, we will mainly focus on stable hydroxyl coverages obtained within an interval of water pressure and temperature including the thermal pre-treatment conditions prior to the NMR experiments, thus for temperatures between 700 and 800 K, and P_{H2O} between 10^{-4} bar and 10^{-6} bar. In some instances, for the sake of trend analysis, we also report results for facets at 400 K and $P_{H2O} = 10^{-2}$ bar, that exhibit higher hydroxyl coverages. The protocol for the simulation of properties such as hydration and chlorination energies, and NMR chemical shift will be described throughout the text and in the **supporting information SI 3 to 5**. Free energy calculations were performed to deduce which hydroxyl coverage leads to the most stable edges for given temperature and water partial pressure conditions, as explained in the **supporting information SI. 6**.

III. Results and discussion

III.1 Non chlorinated sample

The one-dimensional (1D) proton spectrum of the non-chlorinated dehydroxylated γ–alumina sample (**Figure 1 a**) shows characteristic features that were previously analyzed by us as follows.[42] The well resolved peak at ≃ 0 ppm was assigned to μ_1 hydroxyls mainly located on one type of edge of γ-Al_2O_3 crystallites, the so-called (110)/(100) edge (the only one available at that time). Several resonances within an intense massif in the 1-3 ppm range were assigned to μ_1 and μ_2 hydroxyls (with their proton free from H-bonding), located either on facets or edges. A broad component ranging from 3 to 7 ppm corresponds to μ_1, μ_2 or μ_3 hydroxyls with H-bond donors.

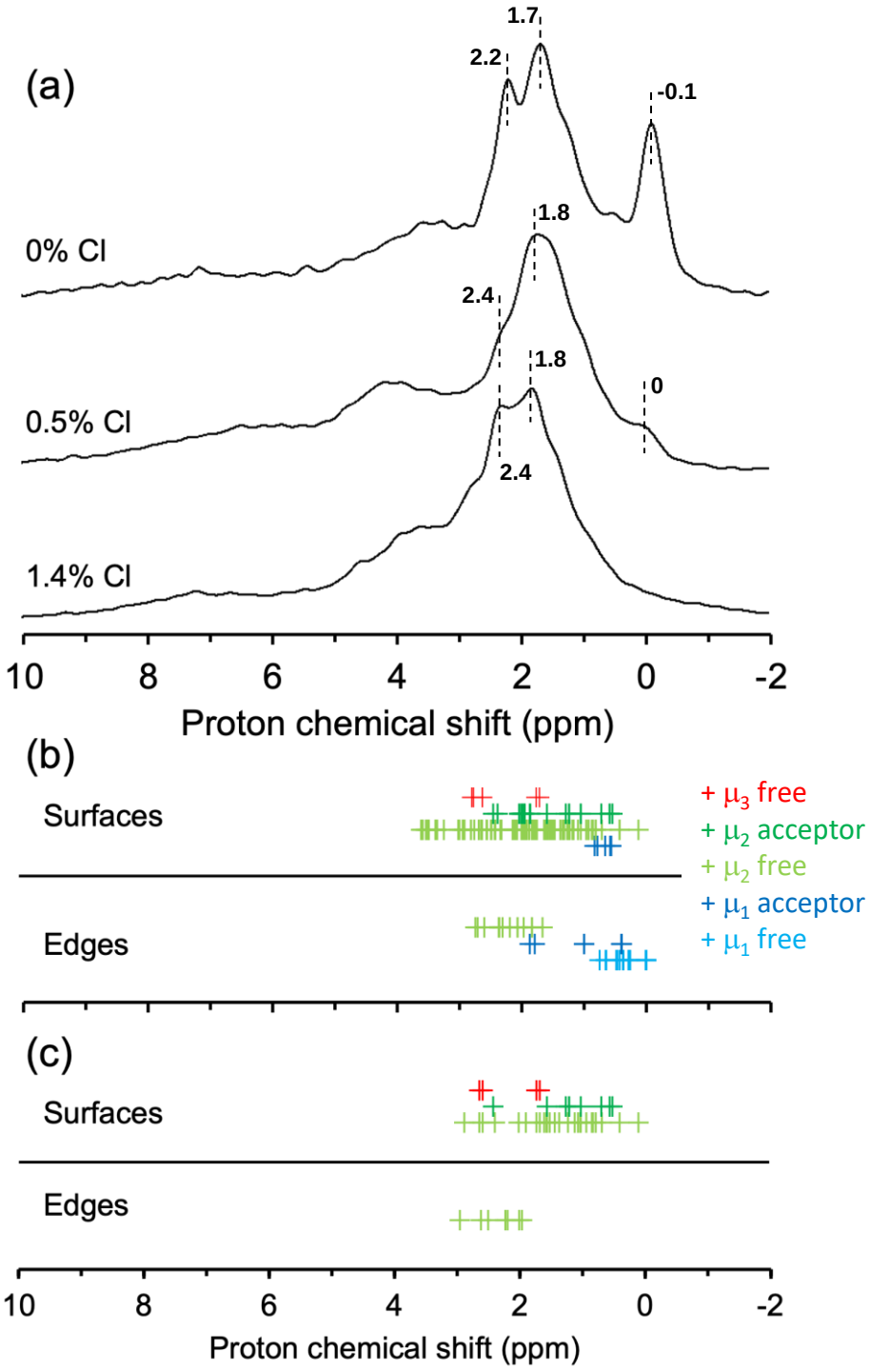
(a)
1.7
2.2
-0.1
0% Cl
1.8
2.4
1.8
0
0.5% Cl
2.4
1.4% Cl
10
8
6
4
2
0
-2
Proton chemical shift (ppm)
(b)
Surfaces
Edges
+ μ3 free
+ μ2 acceptor
+ μ2 free
+ μ1 acceptor
+ μ1 free
(c)
Surfaces
Edges
10
8
6
4
2
0
-2
Proton chemical shift (ppm)

Figure 1. One-dimensional ^{1}H spectra of the of the γ–alumina samples for different chlorine contents. The spectra were recorded using a DEPTH experiment to suppress probe background (a). DFT calculated ^{1}H chemical shifts of free and H-bond acceptor on different facet and edge models before chlorination (b) and after chlorination (c). The models chosen are the most stable ones in the conditions of the experiments.

Figure 2 (a) shows the 2D ^{1}H-^{1}H DQ-SQ spectrum recorded on the non-chlorinated dehydroxylated γ–alumina. The correlations observed in this spectrum allow the identification of proximities between dipolar-coupled protons. Auto-correlation peaks observed along the diagonal (δ_A, $2\delta_A$) correspond to proximities between protons of the same chemical shift, while off-diagonal peaks at (δ_A, $\delta_A+\delta_B$) and (δ_B, $\delta_A+\delta_B$) correspond to two closely spaced protons with different chemical shifts. The intensity of the correlation peaks is modulated by the ^{1}H-^{1}H distance: an intense correlation reflects a close proximity between two protons (typically distances shorter than 5 Å). A significant autocorrelation is observed for protons at -0.1 ppm, reflecting proximities between μ_1 hydroxyls located on edges (to be discussed later). A strong and broad autocorrelation is also observed for the proton resonances at around 1.7 ppm, corresponding to the most intense signal in the 1D spectrum. In addition, two off-diagonal correlations are identified: first between protons at ≃-0.1 ppm and ≃1.9 ppm and second, between protons at ≃2.1 and ≃3.1 ppm. Based on our previous assignment,[42] the first correlation may correspond to proximities between μ_1-OH protons located on edges and other types of hydroxyls (to be identified), while the second one remains to be elucidated. To further interpret these data, DFT calculations were used to determine the local structures and proton chemical shifts of hydroxyl groups located on γ–alumina's facets and edges.

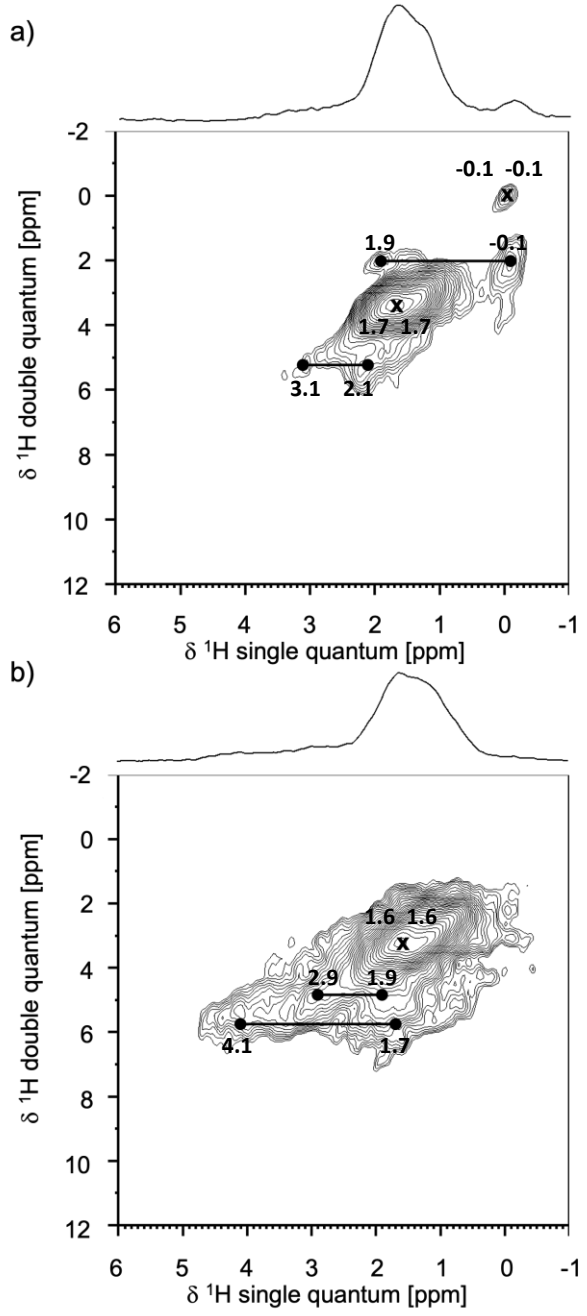

Figure 2. Two-dimensional ^{1}H-^{1}H DQ-SQ spectra of the γ–alumina samples: non chlorinated reference (a), γ–alumina chlorinated at 0.5 wt% Cl (b). Black horizontal lines depict off-diagonal correlations while crosses indicate auto-correlations. The top traces correspond to the projection of the 2D spectra along the single-quantum dimension.

As aforementioned, assuming the transformation of the boehmite particles is topotactic, meaning the overall shape of the particle is conserved during the calcination, the γ–alumina facets are inherited from those of boehmite, thus facets models at the various possible hydroxyl coverages were constructed according to the method proposed in ref.44. **Figure 3** illustrates a hypothetical γ–alumina crystallite highlighting the facets and edges simulated in the present work. The most stable hydroxyl coverages obtained within the relevant interval of water pressure (**Section II.3**) are reported in **Table S4**. The γ–alumina (110) facet inherited from the boehmite (010) facet is defined as the basal (110) and labelled $(110)_b$ (**Figure S6)**. The one inherited from the (100) boehmite surface is called the lateral $(110)_l$ for which four competing models (according to the position of Al tetrahedral sites) were proposed and labelled as $(110)_l$-A1, $(110)_l$-A2, $(110)_l$-L1 and $(110)_l$-L2 (**Figures S7-S10**). In addition, several models were also found for the (111) facets labelled as (111)-D1, (111)-D2 and (111)-P1_2 (**Figures S11-S13**). The various types of Al_{IV}-μ_1-OH stable in experimental conditions are reported in **Table S5**, while all μ_n-OH species are described in **Tables S6-S13**.

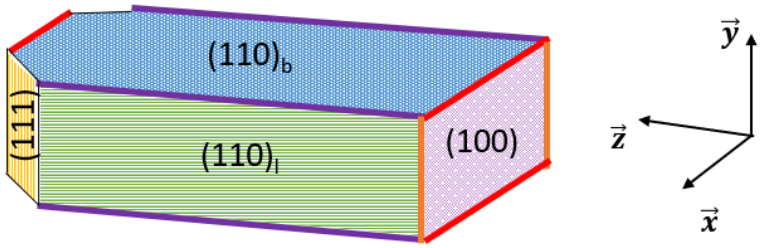

Figure 3. Scheme of a hypothetical γ-alumina crystallite showing all the modelled facets simulated here. The corresponding modelled edges are presented in purple, orange and red thick lines. The system of axes is taken from boehmite using the *Cmcm* space group. The morphology of the

illustrated crystallite does not correspond to a real observed morphology: it is used only for representing the various modelled facets and edges. The right-hand part neglects the existence of the (111) facet that is accounted for in the left-hand part.

In the same spirit as in our previous study,[42] the various kinds of protons were classified into four families, depending on the hydrogen-bond nature around the considered proton: free (no H-bond), H-bond donor, H-bond acceptor (meaning the oxygen atoms covalently bonded to this hydrogen is H bond acceptor) and H-bond acceptor *plus* donor (some protons are indeed both at the same time). To define whether the H atom is involved in a H-bond, we used a distance threshold of 2.5 Å: if the distance between the H donor and the O acceptor is smaller than 2.5 Å, we will assume that a H-bond exists. To make the bridge with NMR experiments, proton chemical shifts are computed according to the methodology of the Gauge Including Projector Augmented Wave (GIPAW) method[61,62] for all facet models (**supporting information SI 5)**. In the case of the $(110)_I$-A1 facet, **Figure S21** clearly shows that the chemical shift of H-bond donor protons is significantly increased in an almost linear way as a function of the OH---O distances. This trend obviously influences the position of all hydroxyl types but in particular μ_1-OH, which are shifted to significantly positive values with respect to the observed peak at 0 ppm, in line with previous analyses.[42,63,64] As illustrated by the extended chemical shift range calculated for the H-bond donors calculated for all different facets (**Figures S22-S28** and **Tables S6-S12**), a very broad chemical shift distribution is expected for these protons.

We then focus on hydroxyls which are either H-bond acceptor or free from H-bonds. **Figure 1 (b)** reports the DFT values of ^{1}H chemical shifts for free and H-bond acceptor located on all the hydroxylated facet models corresponding to experimental conditions. The two main resonances

(at ≃1.7 and ≃2.2 ppm) observed in the ^{1}H NMR spectrum of non-chlorinated γ-alumina correspond predominantly to protons of μ_2-OH species. According to the DFT calculations, the μ_2-OH species (either free or acceptor) spread over a rather large range of chemical shifts from 0 to 3.5 ppm. These μ_2-OH groups could be located on all facets studied here: either $(110)_l$, or $(110)_b$ or (111) facets. The (100) facet is completely dehydrated in experimental conditions. Considering the revisited facet models,[44] it appears that some μ_3-(Al_{VI}-Al_{VI}-Al_{VI})-OH species located on the $(110)_l$-L1 and $(110)_l$-L2 could also contribute to the 2.6-2.8 ppm region, while some on the (111)-P1_2 are predicted to appear at 1.7 ppm. This result enriches our previous work,[42] where the chemical shifts of protons of μ_3-OH of the $(110)_l$-A1 facet were found to be displaced to significantly higher values due to H-bonds.

The 0 ppm peak was generally attributed to μ_1-OH species.[19] However, the structures of the facets containing μ_1-OH groups illustrated in **Figures S6 to S13** reveal that most of these hydroxyls present on the facet models are generally involved in the H-bond network with the exception of the one located on the $(110)_l$-A2 facet model (**Figure S8**). Hence, their calculated chemical shifts spread over a broad range beyond 1 ppm, as illustrated for the $(110)_l$-A1 facet in **Figure S21**. Only, one acceptor μ_1-OH species located on the $(110)_l$-A2 facet exhibits a ≃0.5 ppm shift at 700 K vanishing at 800 K (**Table S7**). Even if we consider the highest temperature (800 K) and lowest water pressure (10^{-6} bar), most of the γ–alumina facets do not contain any stable free μ_1-OH species but rather μ_2- or μ_3-OH species (**Tables S5-S9** and **S12**). None of these species provide ^{1}H chemical shift close to 0 ppm as observed in the ^{1}H DEPTH spectrum, excepting some μ_2-OH species present on the (111)-P1_2 facet model (**Table S13**). This trend partially contradicts the recent assignment proposed by Merle et al.[39] who proposed that the Al_{IV}-μ_1-OH group present on the (110) facet at low OH coverage was able to explain this NMR signal. According to ref.44 the

same $(110)_l$-A1 facet exhibits either strongly donor μ_1-OH, at high coverage, or only μ_2-OH stable at low coverage (**Table S6**). The (111)-D1 and (111)-D2 facets are the only ones to keep one stable Al_{IV}-μ_1-OH (**Tables S11** and **S12**) at 800 K. Due to their still large hydroxyl coverages, the residual H-bond network induces a significant shift beyond 1.7 ppm. This analysis undertaken on a great variety of γ–alumina facets, strengthens our previous proposal[42] that hydroxyls located on facets contribute only marginally to the ≃0 ppm proton resonance.

Hence, free μ_1-OH located on edges deserve a deeper investigation to interpret the experimental data. For that purpose, we simulate the hydration and dehydration of 4 relevant edges $(110)_b$/(100), (100)/$(110)_l$-A1, $(110)_b$/$(110)_l$-A1, $(110)_b$/$(110)_l$-L1 by systematic DFT calculations of Gibbs free energies in the relevant (T, P) conditions (**supporting information SI 6). Table S5** reports the exhaustive list of Al_{IV} edge sites which bear μ_1-OH groups, revealing that the great majority is free of H-bonding. The structures of all simulated edges are illustrated in **Figures S14 to S20**. The structural analysis showed that the $(110)_b$/$(110)_l$-A1 and $(110)_b$/$(110)_l$-L1 edge models exhibit almost the same Al edge sites, illustrated in **Figures S17** to **S20**. In both cases, at temperatures higher than 700 K and water pressure lower than 10^{-2} bar, the edge $Al_{IV\text{-}Td}$-OH are not H-bond donors and may explain the ^{1}H NMR peak at ≃0 ppm (as detailed below). The second key feature of these edges is the existence of Lewis Al_V sites (labelled as α, β, γ, λ, χ in **Figures S17** to **S20** and **Tables S15-S16**). The presence of such Lewis acid sites in a close vicinity to the edge $Al_{IV\text{-}Td}$-OH is something unique to these edge models.

The newly determined $(110)_b$/(100) edge model (**Figure S16**) is rather similar to the already published (100)/$(110)_l$-A1 model (**Figures S14-S15**), the major difference being that $Al_{IV\text{-}Td}$-OH species are present on the two different edges of our nano-rod models (**Figure S4**).

The calculated values of ^{1}H chemical shifts for all protons of these edges are reported in **supporting information SI 7** and summarized in **Table S21** and **Figure 1 (b)** which reveals that most of the chemical shifts of "free" protons located on $Al_{IV\text{-}Td}$-OH at edges are in the range from -0.1 to 0.9 ppm. Those edge $Al_{IV\text{-}Td}$-OH species are thus the best candidates explaining the observed peak at ≃0 ppm in the ^{1}H DEPTH spectrum.

Regarding the μ_2-OH species located at edges, they are all free from H-bond and are located in a narrow interval of chemical shifts between 1.6 and 2.7 ppm, without overlapping with free μ_1-OH (**Figure 1 b**). No μ_3-OH species are located on the edge of our models. Nevertheless, this conclusion should not be considered as strict because this assignment may depend on the definition of the edge region: some μ_3-OH groups could be indeed located on facets at a very near position to edge even if not reported in **Figure 1 (b)**. Analyzing the DFT values of chemical shifts undertaken on all edges and facets, it appears that the DFT dataset is dominated by a major contribution of protons belonging to μ_2-OH species followed by protons of μ_1-OH types and then by minority protons of μ_3-OH types.

To push further this analysis, we now consider the ^{1}H-^{1}H DQ correlation spectrum recorded on the non-chlorinated γ-Al_2O_3 in an attempt to identify correlations involving those protons (**Figure 2 a**). A close examination of the molecular models of the various facets and edges should indeed allow the assignment of the through-space correlations observed in the 2D spectrum, assuming that the distances for ^{1}H-^{1}H correlations are within the 2.5 to ≃5.5 Å range. To circumvent the question of the dynamic behavior of protons (which would require too computationally demanding ab initio molecular dynamics), we approximate the mean ^{1}H-^{1}H distances by the O-O distance between O atoms of the corresponding hydroxyl groups (**Table S14)** instead of considering directly the frozen ^{1}H-^{1}H distances in the 0 K optimized structures. **Table S14** and **Table S21**

reports the pairs of μ_2-OH and/or μ_3-OH protons whose ^{1}H chemical shifts are in the range of the experimental ones and for which the approximate H-H distances are comprised between 2.7 and 4.8 Å.

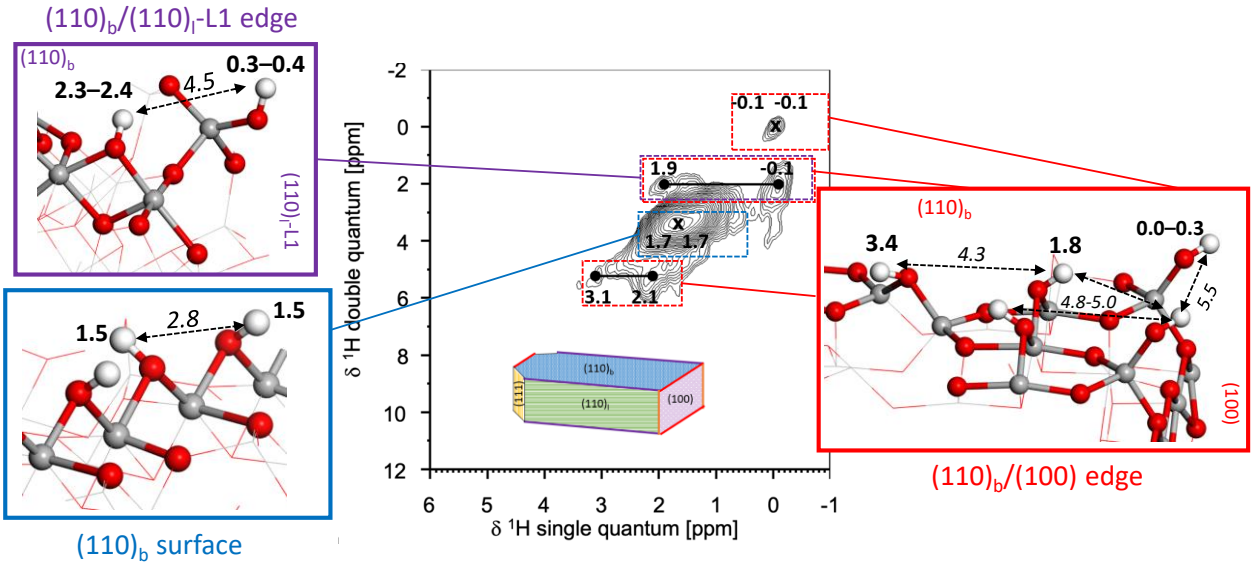

Figure 4: Most relevant hydroxyls proposed to interpret the correlations observed in the ^{1}H-^{1}H double-quantum spectrum of the non-chlorinated γ-Al_2O_3 sample. Chemical shifts (in ppm) are reported as bold numbers, distances (in Å) in italic. Colors of frames are consistent with those of facets represented in the crystallite recalled in the insert.

According to **Table S14**, three facet models $(110)_b$, $(110)_l$-L1 and $(110)_l$-L2 exhibit free μ_2-OH groups at a close distance of each other (2.8 Å). Among these, the most relevant one is the $(110)_b$ facet of which μ_2-OH proton chemical shifts at 1.5-1.6 ppm perfectly matching the main auto-correlation peak observed in the DQ spectrum (**Figure 4**). This agreement confirms the relevance of this recently discovered model of the alumina basal $(110)_b$ facet inherited from the boehmite (010) facet.[44] While this close proximity between μ_2-OH groups was already observed in former NMR studies,[19] the precise location of the hydroxyls had never been identified on this facet so far.

Moreover, the relatively weak auto-correlation at ≃0 ppm in the ^{1}H-^{1}H DQ spectrum is well explained by the proximity between free Al_{IV}-μ_1-OH located at edges (**Table S21**). Numerous pairs of Al_{IV}-μ_1-OH exist on the various edges, while this auto-correlation is best assigned to the Al_{IV}-μ_1-OH located on the $(110)_b$/(100) edge for which the ^{1}H chemical shifts lie in the 0-0.3 ppm range with an average inter-nuclear distance of 5.5 Å (**Figure 4**). This distance is larger than the one involving the μ_2-OH located on the $(110)_b$, which likely explains why this auto-correlation is less intense than the one observed for the μ_2 protons. A second possible assignment would be the Al_{IV}-μ_1-OH species located on the (100)/$(110)_l$-A1 edge model (**Figures S14**) for which the inter-proton distance is 4.2 Å, although the calculated chemical shifts (0.6-0.9 ppm) deviate slightly from the experimentally observed value of ≃0 ppm. Notably, on the $(110)_b$/$(110)_l$-L1 and $(110)_b$/$(110)_l$-A1 edges, the free Al_{IV}-μ_1-OH species are distant from about 8 Å between each other which may be too far to be visible on the ^{1}H-^{1}H DQ spectrum, although this cannot be fully excluded.

The cross-correlations observed in the ^{1}H-^{1}H DQ spectrum for the peaks at -0.1 to 1.9 ppm can be best assigned to protons located in the $(110)_b$/(100) edge providing an optimal configuration with free Al_{IV}-μ_1-OH and ($Al_{VI}Al_{VI}$)-OH-μ_2 groups at a distance of 4.8 Å to each other and with compatible chemical shifts (in the 0.0-0.3 and 1.8-2.1 ppm ranges respectively, **Figure 4**). These cross-correlations could also be explained by the $(110)_b$/$(110)_l$-A1 and $(110)_b$/$(110)_l$-L1 edges (**Table S21)** involving other pairs of free Al_{IV}-μ_1-OH group and (AlAl)-μ_2-OH at a distance of 4.5 Å (**Figure 4**). Here we note that this multiple assignment would be consistent with Recoupling-Time-Encoded ^{1}H{^{27}Al} D-HMQC and proton DQ NMR experiments recently reported on needle-shaped nanocrystals of alumina,[43] revealing distinct types of close-by Al_{IV}-μ_1-OH and (AlAl)-μ_2-OH groups as illustrated by the various local structures found on the DFT models (**Figure 3**).

Finally, the 2.1 and 3.1 ppm correlation peaks could reasonably originate from the ($Al_{VI}Al_{VI}$)-μ_2-OH and ($Al_{IV}Al_{IV}$)-μ_2-OH located near the edge of the $(110)_b$/(100) edge, at a distance of 4.3 Å from each other and with calculated chemical shifts at 1.8 and 3.4 ppm (**Table S21** and **Figure 4**).

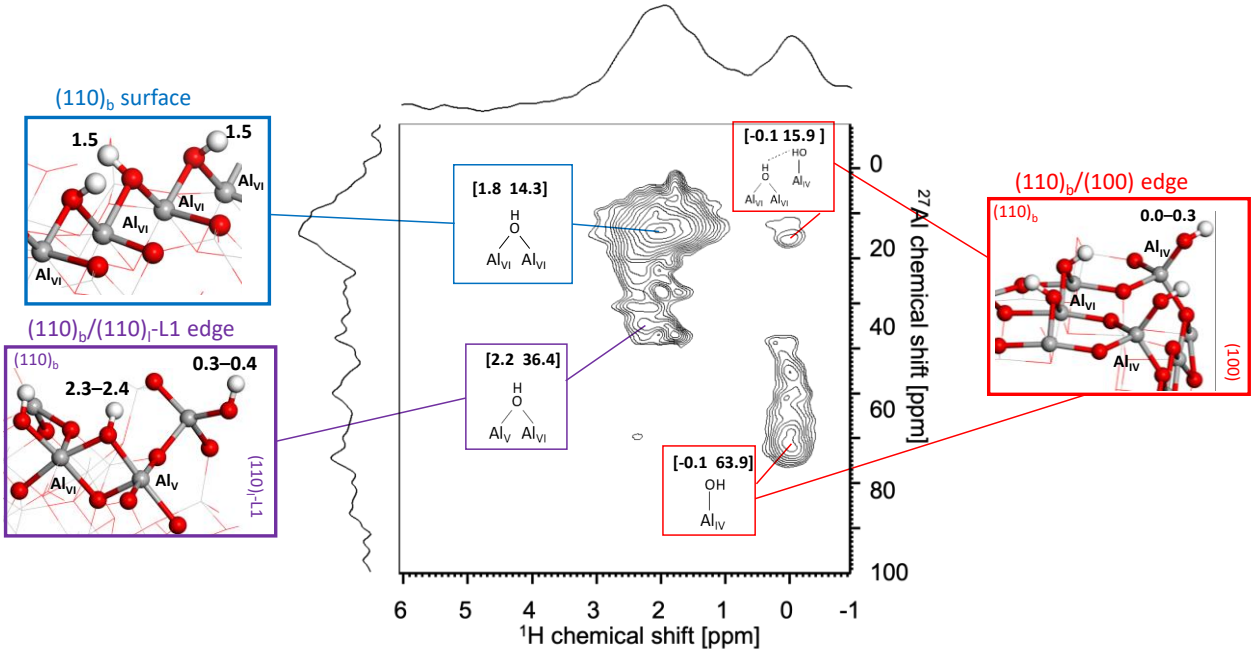

Figure 5 $^1H\{^{27}Al\}$ D-HMQC MAS NMR spectrum of the non-chlorinated γ–alumina sample. The assignment of the correlations to the most relevant hydroxyls and aluminum sites according to the DFT calculations is shown. Chemical shifts (ppm) are reported in bold. Colors of frames are consistent with those of facets of the alumina crystallite represented in **Figure 3**.

The two-dimensional $^1H\{^{27}Al\}$ D-HMQC spectrum of the non-chlorinated γ–alumina sample (**Figure 5**) is coherent with previously reported data on similar samples.[19,43] The most intense correlation at around (δ_{1H}, δ_{27Al})=(1.8 ppm, 14.3 ppm) likely corresponds to various types of protons identified by our DFT calculations. Among the most probable species, μ_2-OH protons connected to two Al_{VI} on the $(110)_b$ facet are providing coherent chemical shifts in the 1.5-1.6 ppm

range, confirming the key role of the basal facet model derived here from the boehmite (010) basal facet in data interpretation.[44] Regarding the second correlation at around (δ_{1H}, δ_{27Al})=(2.2 ppm, 36.4 ppm), the best matches are found for μ_2-OH species (stable at 800 K) connected to mixed (Al_{VI}, Al_V) sites located on the $(110)_b/(110)_l$-L1 edge with ^1H chemical shifts at 2.3-2.4 ppm. μ_2-OH species of the $(110)_b/(110)_l$-A1 edge are also compatible (**Table S21**). Also, the (Al_{VI}, Al_V)-μ_2-OH species may contribute to a correlation around (δ_{1H}, δ_{27Al})=(2.2 ppm, ≃14 ppm) which is hidden in the shoulder of the previous (δ_{1H}, δ_{27Al})=(1.8 ppm, 14.3 ppm) correlation.

Note that a contribution of the $(100)/(110)_l$-A1 edge where μ_2-OH species at 2.5 ppm are connected with (Al_V, Al_V) sites, cannot be excluded although this computed proton chemical shift value slightly overestimates the experimental one. The second most intense correlation at (δ_{1H}, δ_{27Al})=(-0.1 ppm, 63.9 ppm) can be readily assigned to the Al_{IV}-OH species located at edges as described above. The correlation at (δ_{1H}, δ_{27Al}) = (-0.1 ppm, 15.9 ppm) implies a spatial connectivity between μ_1-OH species and Al_{VI} sites. According to previous DFT calculations,[27,44] μ_1-OH hydroxyls located on octahedral Al sites could be stabilized on the (100) facet and some (111) facets at lower temperature (400 K) and higher vapor pressure than the used experimental ones. However, these OH are involved in H-bonds and cannot explain the observed correlation.

III.2 Effect of chlorine

To better understand the influence of chlorination on the structure of γ-Al_2O_3, high-resolution ^{27}Al NMR spectra were recorded on the non-chlorinated and chlorinated γ-Al_2O_3 (**Figure 6**). The spectrum obtained for the pristine γ-Al_2O_3 displays the characteristic features of alumina.[65,66] Three major peaks are observed, centered at 12.9, 33 and 71.9 ppm, and assigned to Al^{3+} cations in octa-, penta- and tetrahedral coordination, respectively. The intensity ratios of Al_{VI}/Al_V and

Al_{VI}/Al_{IV} (at 64.4/2.0 and 64.4/33.6) are typical for γ-Al_2O_3 materials, and reflect the composition of the bulk.[9] Note that this is in contrast with the $^{1}H\{^{27}Al\}$ D-HMQC spectrum which magnify Al(-OH) surface signals (due to edge or facet effects), hence the chemical shifts differences observed between the ^{27}Al spectra of γ-Al_2O_3 in **Figures 5** and **6**. The chlorinated samples show similar spectral features to those observed for the non-chlorinated γ-Al_2O_3. However, an additional shoulder at 78.6 ppm is observed which reveals a structural evolution of the local environment of Al_{IV} sites. Remarkably, similar deshielding has been previously observed for organometallic compounds containing $Al(O)_n(Cl)_m$ anions with increasing number of Cl coordinated to Al.[67] We will also come back to this with DFT calculations.

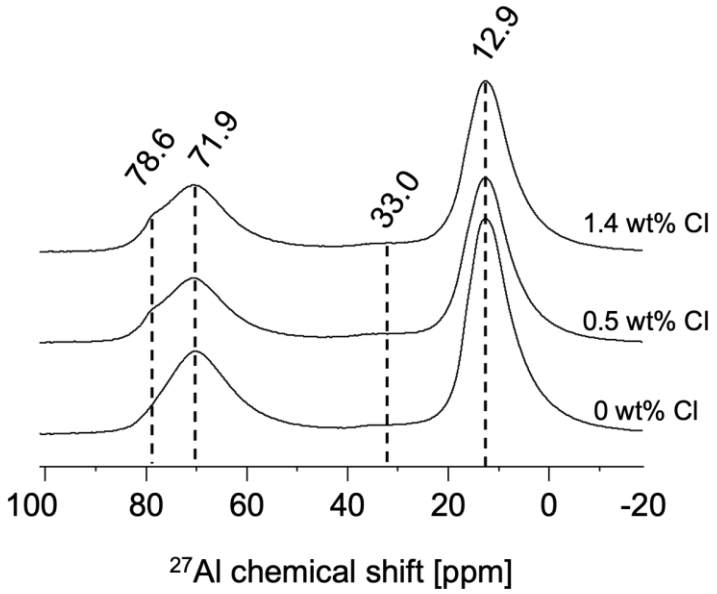

Figure 6. One-dimensional ^{27}Al NMR spectra recorded for γ-Al_2O_3 for three Cl contents: 0 wt% Cl, 0.5 wt% Cl and 1.4 wt% Cl.

One of the main effects of adding chlorine on γ–alumina is the disappearance of the 0 ppm signal on the ^{1}H NMR spectrum (**Figure 1 a**), as previously reported in literature.[15,16,39,42] It can also be underlined that only for the 1.4 wt% Cl loading, the 0 ppm signal vanishes completely, while at 0.5 wt% Cl some μ_1-OH remain present at edges as previously discussed in refs.42,68 The impact of chlorine addition on the ^{1}H-^{1}H DQ spectrum is more complex **(Figure 2 b**). In this case, for 0.5 wt% Cl, the auto- and cross-correlations involving the -0.1 ppm signal are no longer present. Since in ^{1}H NMR spectrum, the -0.1 ppm peak is still present, this means that the fraction of μ_1-OH remaining at edges is now sufficiently low so that these correlations are not observed. The strong diagonal correlation corresponding to proximities between free μ_2 hydroxyls likely located on $(110)_b$ facet of the crystallite, as well as the off-diagonal correlations assigned to close contacts between μ_2 hydroxyls in $(110)_b$ and (100) facets, as elucidated above, are preserved, although slight shifts towards lower chemical shift values are observed. An additional correlation is clearly visible between signals at ≃1.7 and 4.1 ppm on the DQ spectrum of the 0.5 wt% Cl sample.

In order to provide a precise interpretation for this spectral feature, it is first necessary to determine which hydroxyls are thermodynamically exchanged with Cl on the relevant γ-Al_2O_3 facets and edges, and how chlorination disturbs the hydroxyls network and subsequently proximities among μ_n-OH families. Previous DFT, NMR and IR spectroscopic studies on the chlorination of γ-Al_2O_3 models[18,26,42] have shown that μ_1-OH groups are the most labile and preferentially exchanged protons on both facets and edges. Hence, in the present study, only terminal μ_1-OH hydroxyl groups were considered for Cl exchange (**supporting information SI 4)**. **Table S5** reports the exhaustive energetic screening of 29 sites located either on facets or on edges which are summarized in **Figure 7**. The overall screening reveals that 16 out of 17 edge sites exhibit negative exchange energies, many of them being smaller than -30 kJ mol^{-1}. They are distributed on almost

all edges tested. By contrast, only 8 out of 12 facet sites exhibit negative energies, and only two of them are smaller than -30 kJ mol^{-1}, located predominantly on the lateral $(110)_l$ facets. The more difficult chlorination of the $(110)_b$ and (111) facets (**Figure S6** and **Figures S11-S13**) results from the fact that terminal hydroxyls present at the facet are engaged in dense hydrogen bonding networks, where each hydroxyl is simultaneously H-donor and H-acceptor (see also complementary analysis in **supporting information SI 4**). For instance, on the $(110)_b$ facet, the linear chain of H-bonds prevents Cl exchange (**Figure S6**), while the exchanged hydroxyls on the $(110)_l$ are less interconnected (**Figures S7-S10**).

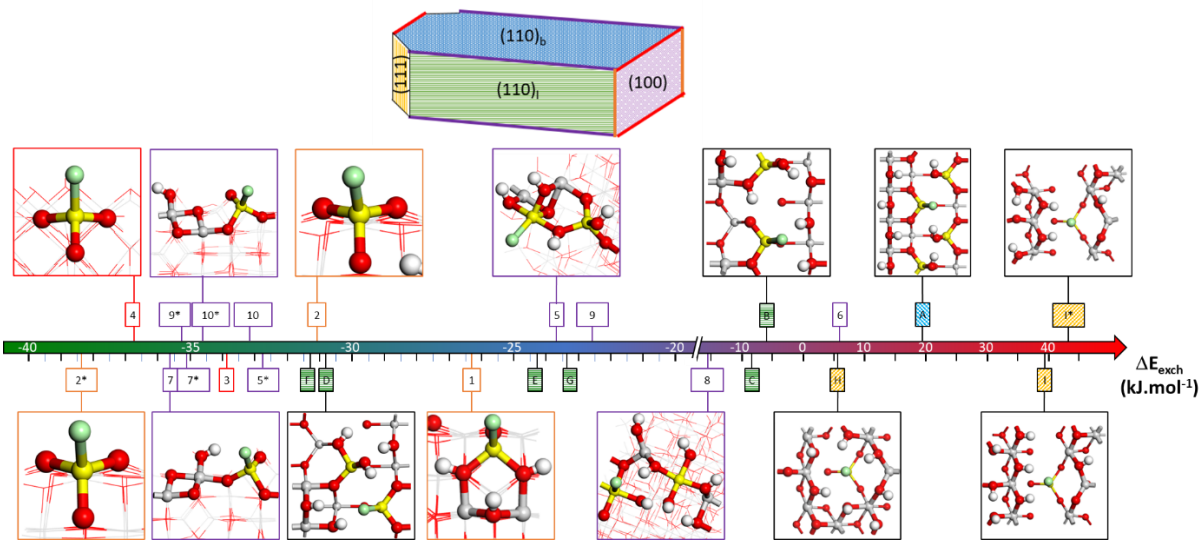

Figure 7. Energy scale for all Cl exchanges with μ_1-OH of the γ-Al_2O_3 facets and edges investigated in this work. Site number, letter coding and numerical values refer to **Table S5**, with frames' colors corresponding to the ones used in the crystallite inset: purple line for $(110)_b/(110)_l$ edge, orange line for $(100)/(110)_l$ edge, red line for $(110)_b/(100)$ edge, green stripes for $(110)_l$ facet, blue stripes for $(110)_b$ facet and yellow stripes for (111) facets. A selection of top or side views of

chlorinated surfaces is given. Color coding for atoms: red-oxygen; grey-aluminum; yellow-aluminum connected to μ_1-OH which can be substituted by Cl; white-hydrogen; green-chlorine.

We discuss here only two cases of edge chlorination, the exhaustive description of each edge being provided in **supporting information SI 4**. Considering the edge formed between the (100) facet with the $(110)_b$ facet, only two inequivalent μ_1-OH are present on each side of the edge supercell. The dehydroxylation temperatures (700 K and 800 K) led to the same thermodynamically stable model as presented in **Figure 8 a**. The exchange of these terminal OH by Cl is an exothermic process with -33.9 kJ.mol^{-1} for site (3) and -36.7 kJ.mol^{-1} for site (4).

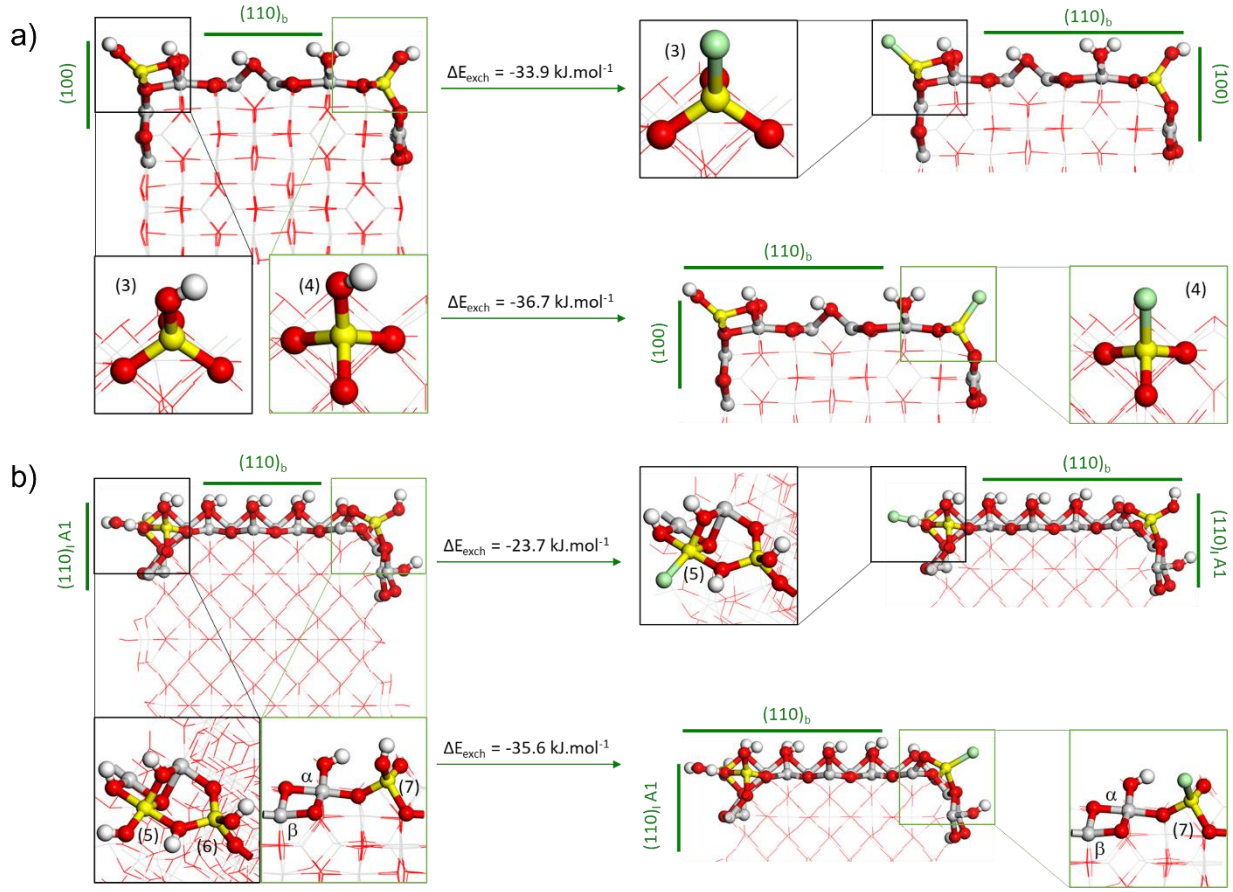

Figure 8: Edge model for the $(110)_b$/(100) at 700 K before (left) and after (right) substitution of μ_1-OH (3 and 4) by Cl (a). Edge model for the $(110)_b$/$(110)_l$ A1 at 700 K before (left) and after

(right) substitution of μ_1-OH (5 and 7) by Cl (b). The dotted blue line indicates hydrogen bonding between OH···O(H). Insets represent zoomed local structures of interest after Cl substitution. Color coding for atoms: red-oxygen; grey-aluminum; yellow-aluminum connected to μ_1-OH which can be substituted by Cl; white-hydrogen; green-chlorine.

For the edge between the lateral $(110)_l$ and the basal $(110)_b$ facets, three possible sites of exchange are present for the dehydroxylation at 700 K and two for the one at 800 K (**Figures 8 b**, **S17-S18**, respectively). For the higher hydroxyl coverage, two μ_1-OH are present at one side of the edge structure while only one is present on the other side. Substitution of site (5) with Cl leads to an exothermic reaction (-23.7 kJ mol^{-1}) indicating a favorable exchange whereas substitution of the second site (6) is slightly endothermic (+5.9 kJ mol^{-1}). This large energy difference between the two sites is due to the local surrounding of site (6) located at the border of the $(110)_b$ facet (**Figure S17**). Site (6) is engaged in hydrogen bonding (H-donor with μ_1-OH and H-acceptor with μ_2-OH) with the terminal hydroxyls present on the $(110)_b$ facet. This interaction is reminiscent of the hydrogen bonding chain between the μ_1-OH groups of the $(110)_b$ facet. By contrast, the other terminal OH (site 7) is not engaged in a hydrogen-bonding network with the $(110)_b$ facet, leading to an exothermic energy of exchange for the Cl substitution of -35.6 kJ mol^{-1}. The thermodynamically stable edge model dehydroxylated at 800 K exposes only two μ_1-OH groups, potential candidates for the Cl exchange (**Figure S18**). For site (7*****), the energy of exchange is in the range of previously calculated values for μ_1-OH present on the edge of γ-Al_2O_3, with -35.1 kJ mol^{-1}.

For the chlorinated facets and edges, ^{27}Al and ^{1}H NMR calculations were performed to interpret the spectral changes observed upon chlorination. For the tetrahedral aluminum bearing the μ_1-OH

substituted by Cl, a clear displacement towards higher values of the ^{27}Al chemical shift is revealed by DFT calculations. The average difference between Al_{IV}-Cl and its Al_{IV}-μ_1-OH counterpart is evaluated at 6.6 and 12.4 ppm for facets and edges, respectively (**Table S22**). These two calculated chemical shift changes are qualitatively consistent with the experimental ^{27}Al MAS NMR described above. Indeed, the ^{27}Al chemical shift value of 63.9 ppm obtained from ^{1}H{^{27}Al} D-HMQC (**Figure 5**) for the surface Al_{IV} site located on edges and directly connected to the μ_1-OH species, is significantly smaller than the one corresponding to the resonance of the aluminum exchanged by Cl and which appears at around 78.6 ppm in **Figure 6**. Although these values do not correspond to true chemical shifts (as the contribution of the quadrupolar coupling shifts the NMR lines), the calculated variation evaluated at ≃14.7 ppm would be in line with the expected effect of the chlorination of Al_{IV} edge site.

Similarly, several features of the 2D ^{1}H-^{1}H DQ spectra of the 0.5 wt% samples can be explained from the DFT models of the chlorinated γ-Al_2O_3 models and chemical shift calculations. First, the partial or complete Cl exchange of the Al-μ_1-OH groups located on the (100)/$(110)_l$-A1 or $(110)_b$/(100) edges and identified as good candidates for the ^{1}H at 0 ppm (site 2*, 3 or 4) correspond to the most favorable substitution enthalpy (-34 < μ_1-Cl < -38 kJ.mol^{-1}) among all edge and facet models. This substitution induces the disappearance of the 0 ppm proton signal and obviously of the corresponding correlations in the 2D DQ spectra. Thus, the cross-correlation at 1.9 and -0.1 ppm, resulting from the interaction of Al_{IV}-μ_1-OH with OH-μ_2-($Al_{IV}Al_{VI}$) or OH-μ_2-($Al_{VI}Al_{VI}$) present on the (100)/$(110)_l$-L1 or $(110)_b$/(100) edges vanishes as expected.

As previously noticed, a slight shielding effect occurs for the protons involved in the main auto-correlation from around 1.7 ppm for the non-chlorinated sample to 1.6 ppm at 0.5 %wt Cl content, as well as for those involved in the cross-correlation with shifts for the pairs of nearby protons

from 2.1 and 3.1 ppm (0 %wt Cl) to 1.9 and 2.9 ppm (0.5 %wt Cl). Moreover, as discussed above, new correlations are observed. These observations may result from the disruption of the H-bond network among hydroxyls which is induced by chlorine exchange with μ_1-OH hydroxyls. For instance, if one considers the DFT facet models of the $(110)_l$-A1 (**Figure S7**), $(110)_l$-A2 (**Figure S8**) and $(110)_l$-L1 (**Figure S9**) and, the μ_2-OH or μ_3-OH species are strong H-bond donors to μ_1-OH neighbors in absence of Cl, which is no longer the case after chlorination. Thus, they could now be revealed in the 2D spectra. As shown in **Figures S7-S9,** the OH bond length of either μ_2-OH or μ_3-OH groups contracts by ≃0.015-0.020 Å which induces a negative displacement of the calculated ^{1}H chemical shift leading to the possible appearance of contributions at lower chemical shifts not present before chlorination.

Conclusions

We provided a combined NMR and DFT investigation of industrially relevant γ–alumina materials. One- and two-dimensional ^{1}H NMR spectra were recorded using high magnetic fields that revealed various types of hydroxyl species featuring distinct and well-defined through-space correlations, sensitive to the chlorine addition (ex-HCl). An exhaustive DFT investigation was undertaken for 8 facet models of γ–alumina. In parallel, 4 edge models were constructed with hydration and chlorination states optimized for two relevant (T, P) conditions in order to allow for comparison with NMR experiments.

This analysis allowed first the assignment of the various ^{1}H resonances as well as of all the spatial connectivities observed experimentally in the pure γ–alumina spectra. To interpret the resonance at ≃0 ppm, the contribution of Al_{Td}-μ_1-OH present on edges where these hydroxyls are free from

H-bonds, was crucial. We show notably that these hydroxyls, when located on the $(110)_b/(100)$ edge, explain nicely the autocorrelation revealed in the ^1H-^1H SQ-DQ experiment. The cross-correlation at -0.1/2.0 ppm is explained by two types of edges: the $(110)_b/(100)$ and the $(110)_b/(110)_l$. Finally, the μ_2-OH present on the $(110)_b/(100)$ edge and on the near edge were shown to be at the origin of the autocorrelation at 1.7 ppm and cross-correlations at 3.1/2.1 ppm. The correlations observed in the $^1H\{^{27}Al\}$ D-HMQC MAS NMR spectrum could also be fully interpreted in the light of these μ_1-OH and μ_2-OH species.

The μ_1-OH exchange with Cl ion provided an atomic-scale understanding of the preferential substitution sites upon alumina chlorination. ^{27}Al NMR reveals a deshielding effect of Al_{Td} induced by the presence of Cl which could be confirmed by DFT calculations. From an energetic point of view, several trends are shown by DFT. The substitutions of μ_1-OH engaged in a dense hydrogen bonding network are energetically disfavored. In particular, the chlorination of lateral (111) and basal $(110)_b$ facets can be ruled out for Cl concentrations used in our experiments. By contrast, the more energetically favored substitutions of free μ_1-OH mainly involved sites present on the edges of the γ-Al_2O_3 crystallite. We cannot exclude that the lateral $(110)_l$ facets (particularly on $(110)_l$-A2, L1 and L2) where the H-bond network is less dense are also chlorinated. This DFT analysis provides a rational interpretation of the disappearance of all the signals in the ^1H DEPTH and ^1H-^1H DQ spectra induced by the free μ_1-OH located on edges after chlorination. We also discussed the subtle changes observed in the NMR experiments after chlorination. It likely results from the disruption of the H-bond network induced by Cl exchange which led to the appearance of signals assigned to μ_2-OH, μ_3-OH free from H-bonds.

With this work, we show that the combination of advanced high-field NMR characterization and state of the art DFT simulation is able to decipher the atomic structure of alumina surface sites and

their proximity in various environments. The large set of calculated ^{1}H chemical shifts corresponding to various hydroxyl configurations located at edges and facets may help in the future for a better assignment of high-resolution NMR spectra of any alumina sample. Moreover, alumina edges have been recently proposed to play a role in the catalytic properties of isolated copper for methane to methanol reaction[5] or in the activation/deactivation mechanisms of silver.[69] Hence, this refined understanding provided in the present work will help to push further the progress in the design and preparation of alumina supported catalysts thanks to a more rational tuning of facets and edges exposed according to the nature of hydroxyl sites targeted.

ASSOCIATED CONTENT

AUTHOR INFORMATION

Corresponding Authors

*E-mail: pascal.raybaud@ifpen.fr

ORCID: Pascal Raybaud : 0000-0003-4506-5062

*E-mail : anne.lesage@ens-lyon.fr

ORCID : Anne Lesage : 0000-0003-1958-2840

Author Contributions

AFTB and TP contributed equally to this paper.

ATFB prepared the samples and performed the TEM analysis. JM, DW, LC and ATFB performed the NMR experiments. TP performed DFT calculations determining the alumina non-chlorinated surfaces and nano-rod models, and chemical shift calculations. JM performed DFT calculations of the chlorinated model systems and chemical shift calculations. ASG, FD, CC and PR designed the

whole study. CC and PR designed the computational study. DW, MR, DG and AL designed the NMR acquisition experiments. The original draft of the paper was written by ATFB, TP, JM and PR with further contributions of all authors. ASG, FD, CC and PR got the funding from the scientific division of IFPEN. PR and AL got the ANR fundings described in the subsequent section. All authors have given approval to the final version of the manuscript.

Funding Sources

This work was supported by the "RatiOnAl Design for CATalysis" (ROAD4CAT) industrial chair, project IDEXLYON funded by the French National Research Agency (ANR-16-IDEX-0005) and the Commissariat-General for Investment (CGI) within the framework of Investissements d'Avenir program ("Investment for the future"). It has also been supported by the Common Research Laboratory "CARactérisation des Matériaux pour l'Energie" CARMEN (ENS deLyon, CNRS, IFPEN, Claude Bernard Lyon 1, University, Sorbonne University, and University of Strasbourg). This work was funded by IFPEN and financial support from Equipex contract ANR-10-EQPX-47-01 is acknowledged. Financial support from the IR INFRANALYTICS FR2054 for conducting the research is gratefully acknowledged.

Supporting Information 1. Alumina sample characterization - 2. Complementary DFT information - 3. Structural models of the γ–alumina facets and edges before and after chlorination. - 4. Nature of OH sites and energetics of the chlorination on facets and edges - 5. Calculated ^{1}H chemical shifts on the γ–alumina facets - 6. Hydration of edge models - 7. Calculated ^{1}H chemical shifts on the γ–alumina edges.

CIF files of the DFT molecular structures of the 4 alumina edges at two experimental conditions are provided as web enhanced objects.

This material is available free of charge via the Internet at http://pubs.acs.org.

ACKNOWLEDGMENTS

Calculations were performed using HPC resources from GENCI-CINES (Grant A0020806134) and from IFP Energies Nouvelles (ENER 440). TGIR RMN THC (FR3050 CNRS) is acknowledged for the NMR characterizations.

REFERENCES

(1) Chen, S.; Wojcieszak, R.; Dumeignil, F.; Marceau, E.; Royer, S.: How Catalysts and Experimental Conditions Determine the Selective Hydroconversion of Furfural and 5-Hydroxymethylfurfural. *Chem. Rev.* **2018**, *118*, 11023-11117.

(2) Larmier, K.; Nicolle, A.; Chizallet, C.; Cadran, N.; Maury, S.; Lamic-Humblot, A. F.; Marceau, E.; Lauron-Pernot, H.: Influence of Coadsorbed Water and Alcohol Molecules on Isopropyl Alcohol Dehydration on Gamma-Alumina: Multiscale Modeling of Experimental Kinetic Profiles. *ACS Catal.* **2016**, *6*, 1905-1920.

(3) Zhang, B.; Xiang, S.; Frenkel, A. I.; Wachs, I. E.: Molecular Design of Supported Moox Catalysts with Surface Taox Promotion for Olefin Metathesis. *ACS Catal.* **2022**, *12*, 3226-3237.

(4) Copéret, C.; Comas-Vives, A.; Conley, M. P.; Estes, D. P.; Fedorov, A.; Mougel, V.; Nagae, H.; Núñez-Zarur, F.; Zhizhko, P. A.: Surface Organometallic and Coordination Chemistry toward Single-Site Heterogeneous Catalysts: Strategies, Methods, Structures, and Activities. *Chem. Rev.* **2016**, *116*, 323-421.

(5) Meyet, J.; Ashuiev, A.; Noh, G.; Newton, M. A.; Klose, D.; Searles, K.; van Bavel, A. P.; Horton, A. D.; Jeschke, G.; van Bokhoven, J. A.; Copéret, C.: Methane-to-Methanol on Mononuclear Copper(II) Sites Supported on Al_2O_3: Structure of Active Sites from Electron Paramagnetic Resonance. *Angew. Chem., Int. Ed.* **2021**, *60*, 16200-16207.

(6) Bara, C.; Plais, L.; Larmier, K.; Devers, E.; Digne, M.; Lamic-Humblot, A. F.; Pirngruber, G. D.; Carrier, X.: Aqueous-Phase Preparation of Model Hds Catalysts on Planar Alumina Substrates: Support Effect on Mo Adsorption and Sulfidation. *J. Am. Chem. Soc.* **2015**, *137*, 15915-15928.

(7) Hoffman, A. J.; Asokan, C.; Gadinas, N.; Schroeder, E.; Zakem, G.; Nystrom, S. V.; Getsoian, A. B.; Christopher, P.; Hibbitts, D.: Experimental and Theoretical Characterization

of Rh Single Atoms Supported on γ–Al_2O_3 with Varying Hydroxyl Contents During NO Reduction by Co. *ACS Catal.* **2022**, *12*, 11697-11715.

(8) Sangnier, A.; Genty, E.; Iachella, M.; Sautet, P.; Raybaud, P.; Matrat, M.; Dujardin, C.; Chizallet, C.: Thermokinetic and Spectroscopic Mapping of Carbon Monoxide Adsorption on Highly Dispersed Pt/γ–Al_2O_3. *ACS Catal.* **2021**, *11*, 13280-13293.

(9) Euzen, P.; Raybaud, P.; Krokidis, X.; Toulhoat, H.; Le Loarer, J. L.; Jolivet, J. P.; Froidefond, C.: Alumina. In *Handbook of Porous Solids*; Wiley-VCH Verlag GmbH, 2008; pp 1591-1677.

(10) Valero, M.C.; Raybaud P.: Computational Chemistry Approaches for the Preparation of Supported Catalysts: Progress and Challenges. *J. Catal.* **2020**, *391*, 539–547.

(11) Knözinger, H.; Ratnasamy, P.: Catalytic Aluminas: Surface Models and Characterization of Surface Sites. *Catal. Rev.* **1978**, *17*, 31–70.

(12) Zecchina, A.; Escalona Platero, E.; Otero Arean, C.: Infrared Characterization of Group Vib Metal Carbonyls Adsorbed On .Gamma.-Alumina. *Inorg. Chem.* **1988**, *27*, 102-106.

(13) Busca, G.: The Surface of Transitional Aluminas: A Critical Review. *Catal. Today* **2014**, *226*, 2-13.

(14) Decanio, E. C.; Edwards, J. C.; Bruno, J. W.: Solid-State ^{1}H MAS NMR Characterization of Gamma-Alumina and Modified Gamma-Aluminas. *J. Catal.* **1994**, *148*, 76-83.

(15) Hietala, J.; Root, A.; Knuuttila, P.: The Surface Acidity of Pure and Modified Aluminas in Re/Al_2O_3 Metathesis Catalysts as Studied by ^{1}H MAS NMR Spectroscopy and Its Importance in the Ethenolysis of 1,5-Cyclooctadiene. *J. Catal.* **1994**, *150*, 46–55.

(16) Kytökivi, A.; Lindblad, M.; Root, A.: IR and ^{1}H NMR Studies on the Adsorption of Gaseous Hydrogen Chloride on γ-Alumina. *J. Chem. Soc., Faraday Trans.* **1995**, *91*, 941-948.

(17) Morterra, C.; Magnacca, G.: A Case Study: Surface Chemistry and Surface Structure of Catalytic Aluminas, as Studied by Vibrational Spectroscopy of Adsorbed Species. *Catal. Today* **1996**, *27*, 497-532.

(18) Digne, M.; Raybaud, P.; Sautet, P.; Guillaume, D.; Toulhoat, H.: Atomic Scale Insights on Chlorinated Gamma-Alumina Surfaces. *J. Am. Chem. Soc.* **2008**, *130*, 11030-11039.

(19) Taoufik, M.; Szeto, K. C.; Merle, N.; Rosal, I. D.; Maron, L.; Trébosc, J.; Tricot, G.; Gauvin, R. M.; Delevoye, L.: Heteronuclear Nmr Spectroscopy as a Surface-Selective Technique: A Unique Look at the Hydroxyl Groups of γ–Alumina. *Chem. Eur. J.* **2014**, *20*, 4038-4046.

(20) Delgado, M.; Delbecq, F.; Santini, C. C.; Lefebvre, F.; Norsic, S.; Putaj, P.; Sautet, P.; Basset, J.-M.: Evolution of Structure and of Grafting Properties of γ–Alumina with Pretreatment Temperature. *J. Phys. Chem. C* **2012**, *116*, 834-843.

(21) Chandran, C. V.; Kirschhock, C. E. A.; Radhakrishnan, S.; Taulelle, F.; Martens, J. A.; Breynaert, E.: Alumina: Discriminative Analysis Using 3d Correlation of Solid-State NMR Parameters. *Chem. Soc. Rev.* **2019**, *48*, 134-156.

(22) Wang, Q.; Li, W.; Hung, I.; Mentink-Vigier, F.; Wang, X.; Qi, G.; Wang, X.; Gan, Z.; Xu, J.; Deng, F.: Mapping the Oxygen Structure of γ–Al_2O_3 by High-Field Solid-State NMR Spectroscopy. *Nat. Commun.* **2020**, *11*, 3620.

(23) Rivet, Q.; Meyet, J.; Rivallan, M.; Nardin, T.; Farrusseng, D.: Characterization of the Brønsted Acidity of $Ptsn/Al_2O_3$ Surfaces by Adsorption of 2,6-Di-Tert-Butylpyridine. *New J. Chem.* **2022**, *46*, 7557-7562.

(24) Zhao, Z.; Xiao, D.; Chen, K.; Wang, R.; Liang, L.; Liu, Z.; Hung, I.; Gan, Z.; Hou, G.: Nature of Five-Coordinated Al in γ–Al_2O_3 Revealed by Ultra-High-Field Solid-State NMR. *ACS Central Science* **2022**, *8*, 795-803.

(25) Khivantsev, K.; Jaegers, N. R.; Kwak, J.-H.; Szanyi, J.; Kovarik, L.: Precise Identification and Characterization of Catalytically Active Sites on the Surface of Γ-Alumina. *Angew. Chem., Int. Ed.* **2021**, *60*, 17522-17530.

(26) Digne, M.; Sautet, P.; Raybaud, P.; Euzen, P.; Toulhoat, H.: Hydroxyl Groups on Gamma-Alumina Surfaces: A DFT Study. *J. Catal.* **2002**, *211*, 1-5.

(27) Digne, M.; Sautet, P.; Raybaud, P.; Euzen, P.; Toulhoat, H.: Use of DFT to Achieve a Rational Understanding of Acid-Basic Properties of Gamma-Alumina Surfaces. *J. Catal.* **2004**, *226*, 54-68.

(28) Lagauche, M.; Larmier, K.; Jolimaitre, E.; Barthelet, K.; Chizallet, C.; Favergeon, L.; Pijolat, M.: Thermodynamic Characterization of the Hydroxyl Group on the γ–Alumina Surface by the Energy Distribution Function. *J. Phys. Chem. C* **2017**, *121*, 16770-16782.

(29) Wischert, R.; Laurent, P.; Copéret, C.; Delbecq, F.; Sautet, P.: γ–Alumina: The Essential and Unexpected Role of Water for the Structure, Stability, and Reactivity of "Defect" Sites. *J. Am. Chem. Soc.* **2012**, *134*, 14430-14449.

(30) Wischert, R.; Copéret, C.; Delbecq, F.; Sautet, P.: Optimal Water Coverage on Alumina: A Key to Generate Lewis Acid-Base Pairs That Are Reactive Towards the C-H Bond Activation of Methane. *Angew. Chem.* **2011**, *123*, 3260–3263.

(31) Pinto, H. P.; Nieminen, R. M.; Elliott, S. D.: Ab Initio Study of γ–Al_2O_3 Surfaces. *Phys. Rev. B* **2004**, *70*, 125402

(32) Ferreira, A. R.; Küçükbenli, E.; de Gironcoli, S.; Souza, W. F.; Chiaro, S. S. X.; Konstantinova, E.; Leitão, A. A.: Structural Models of Activated γ–Alumina Surfaces Revisited: Thermodynamics, NMR and IR Spectroscopies from Ab Initio Calculations. *Chem. Phys.* **2013**, *423*, 62-72.

(33) Larmier, K.; Chizallet, C.; Cadran, N.; Maury, S.; Abboud, J.; Lamic-Humblot, A. F.; Marceau, E.; Lauron-Pernot, H.: Mechanistic Investigation of Isopropanol Conversion on Alumina Catalysts: Location of Active Sites for Alkene/Ether Production. *ACS Catal.* **2015**, *5*, 4423-4437.

(34) Hu, J. Z.; Xu, S.; Kwak, J. H.; Hu, M. Y.; Wan, C.; Zhao, Z.; Szanyi, J.; Bao, X.; Han, X.; Wang, Y.; Peden, C. H. F.: High Field ^{27}Al MAS NMR and TPD Studies of Active Sites in Ethanol Dehydration Using Thermally Treated Transitional Aluminas as Catalysts. *J. Catal.* **2016**, *336*, 85-93.

(35) Carrier, X.; de la Caillerie, J. B. D.; Lambert, J. F.; Che, M.: The Support as a Chemical Reagent in the Preparation of WO_x/γ–Al_2O_3 Catalysts: Formation and Deposition of Aluminotungstic Heteropolyanions. *J. Am. Chem. Soc.* **1999**, *121*, 3377-3381.

(36) Prins, R.: On the Structure of γ–Al_2O_3. *J. Catal.* **2020**, *392*, 336-346.

(37) Chen, C.-H.; Gaillard, E.; Mentink-Vigier, F.; Chen, K.; Gan, Z.; Gaveau, P.; Rebière, B.; Berthelot, R.; Florian, P.; Bonhomme, C.; Smith, M. E.; Métro, T.-X.; Alonso, B.; Laurencin, D.: Direct ^{17}O Isotopic Labeling of Oxides Using Mechanochemistry. *Inorg. Chem.* **2020**, *59*, 13050-13066.

(38) Moroz, I. B.; Larmier, K.; Liao, W.-C.; Copéret, C.: Discerning γ–Alumina Surface Sites with Nitrogen-15 Dynamic Nuclear Polarization Surface Enhanced NMR Spectroscopy of Adsorbed Pyridine. *J. Phys. Chem. C* **2018**, *122*, 10871-10882.

(39) Merle, N.; Tabassum, T.; Scott, S. L.; Motta, A.; Szeto, K.; Taoufik, M.; Gauvin, R. M.; Delevoye, L.: High-Field NMR, Reactivity, and DFT Modeling Reveal the γ–Al_2O_3 Surface Hydroxyl Network. *Angew. Chem., Int. Ed.* **2022**, *61*, e2022073.

(40) Krokidis, X.; Raybaud, P.; Gobichon, A. E.; Rebours, B.; Euzen, P.; Toulhoat, H.: Theoretical Study of the Dehydration Process of Boehmite to Gamma-Alumina. *J. Phys. Chem. B* **2001**, *105*, 5121-5130.

(41) Wischert, R.; Florian, P.; Copéret, C.; Massiot, D.; Sautet, P.: Visibility of Al Surface Sites of γ–Alumina: A Combined Computational and Experimental Point of View. *J. Phys. Chem. C* **2014**, *118*, 15292-15299.

(42) Batista, A. T. F.; Wisser, D.; Pigeon, T.; Gajan, D.; Diehl, F.; Rivallan, M.; Catita, L.; Gay, A. S.; Lesage, A.; Chizallet, C.; Raybaud, P.: Beyond γ–Al_2O_3 Crystallite Surfaces: The Hidden Features of Edges Revealed by Solid-State ^{1}H NMR and DFT Calculations. *J. Catal.* **2019**, *378*, 140-143.

(43) Völker, L. A.; Meyet, J.; Berkson, Z. J.; Rochlitz, L.; van Bokhoven, J. A.; Copéret, C.: Revisiting Edge Sites of γ–Al_2O_3 Using Needle-Shaped Nanocrystals and Recoupling-Time-Encoded {^{27}Al}-^{1}H D-HMQC NMR Spectroscopy. *J. Phys. Chem. C* **2022**, *126*, 6351-6360.

(44) Pigeon, T.; Chizallet, C.; Raybaud, P.: Revisiting γ–Alumina Surface Models through the Topotactic Transformation of Boehmite Surfaces. *J. Catal.* **2022**, *405*, 140-151.

(45) Raybaud, P.; Digne, M.; Iftmie, R.; Wellens, W.; Euzen, P.; Toulhoat, H.: Morphology and Surface Properties of Boehmite (Γ-AlOOH): A Density Functional Theory Study. *J. Catal.* **2001**, *201*, 236-246.

(46) Chiche, D.; Chizallet, C.; Durupthy, O.; Channeac, C.; Revel, R.; Raybaud, P.; Jolivet, J. P.: Growth of Boehmite Particles in the Presence of Xylitol: Morphology Oriented by the Nest Effect of Hydrogen Bonding. *Phys. Chem. Chem. Phys.* **2009**, *11*, 11310-11323.

(47) Bendall, M. R.; Pegg, D. T.: Theoretical Description of Depth Pulse Sequences, on and Off Resonance, Including Improvements and Extensions Thereof. *Magn. Reson. Med.* **1985**, *2*, 91-113.

(48) Cory, D. G.; Ritchey, W. M.: Suppression of Signals from the Probe in Bloch Decay Spectra. *J. Magn. Reson.* **1988**, *80*, 128-132.

(49) Robin Bendall, M.; Gordon, R. E.: Depth and Refocusing Pulses Designed for Multipulse NMR with Surface Coils. *J. Magn. Reson.* **1983**, *53*, 365-385.

(50) Sommer, W.; Gottwald, J.; Demco, D. E.; Spiess, H. W.: Dipolar Heteronuclear Multiple-Quantum NMR Spectroscopy in Rotating Solids. *J. Magn. Reson., Series A* **1995**, *113*, 131-134.

(51) Fung, B. M.; Khitrin, A. K.; Ermolaev, K.: An Improved Broadband Decoupling Sequence for Liquid Crystals and Solids. *J. Magn. Reson.* **2000**, *142*, 97-101.

(52) Venkatesh, A.; Hanrahan, M. P.; Rossini, A. J.: Proton Detection of Mas Solid-State NMR Spectra of Half-Integer Quadrupolar Nuclei. *Solid State Nucl. Magn. Reson.* **2017**, *84*, 171-181.

(53) Brinkmann, A.; Kentgens, A. P. M.: Proton-Selective ^{17}O–H Distance Measurements in Fast Magic-Angle-Spinning Solid-State NMR Spectroscopy for the Determination of Hydrogen Bond Lengths. *J. Am. Chem. Soc.* **2006**, *128*, 14758-14759.

(54) Marion, D.; Ikura, M.; Tschudin, R.; Bax, A.: Rapid Recording of 2D NMR Spectra without Phase Cycling. Application to the Study of Hydrogen Exchange in Proteins. *J. Magn. Reson.* **1989**, *85*, 393-399.

(55) Kresse, G.; Furthmüller, J.: Efficiency of Ab-Initio Total Energy Calculations for Metals and Semiconductors Using a Plane-Wave Basis Set. *Comput. Mater. Sci.* **1996**, *6*, 15-50.

(56) Kresse, G.; Furthmüller, J.: Efficient Iterative Schemes for Ab Initio Total-Energy Calculations Using a Plane-Wave Basis Set. *Phys. Rev. B* **1996**, *54*, 11169-11186.

(57) Perdew, J. P.; Burke, K.; Ernzerhof, M.: Generalized Gradient Approximation Made Simple. *Phys. Rev. Lett.* **1996**, *77*, 3865-3868.

(58) Steinmann, S. N.; Corminboeuf, C.: Comprehensive Bench Marking of a Density-Dependent Dispersion Correction. *J. Chem. Theory Comput.* **2011**, *7*, 3567-3577.

(59) Steinmann, S. N.; Corminboeuf, C.: A Generalized-Gradient Approximation Exchange Hole Model for Dispersion Coefficients. *J. Chem. Phys.* **2011**, *134,* 044117.

(60) Pigeon, T.; Chizallet, C.; Raybaud, P.: Atomic Structures of the Gamma-Alumina Surfaces Are Available on the Nomad Repository & Archive (2021) https://doi.org/10.17172/NOMAD/2021.11.10-1

(61) Pickard, C. J.; Mauri, F.: All-Electron Magnetic Response with Pseudopotentials: NMR Chemical Shifts. *Phys. Rev. B: Condens. Matter* **2001**, *63,* 245101.

(62) Yates, J. R.; Pickard, C. J.; Mauri, F.: Calculation of NMR Chemical Shifts for Extended Systems Using Ultrasoft Pseudopotentials. *Phys. Rev. B* **2007**, *76,* 024401.

(63) Chizallet, C.; Costentin, G.; Lauron-Pernot, H.; Che, M.; Bonhomme, C.; Maquet, J.; Delbecq, F.; Sautet, P.: Study of the Structure of OH Groups on MgO by 1D and 2D ^{1}H MAS NMR Combined with DFT Cluster Calculations. *J. Phys. Chem. C* **2007**, *111*, 18279-18287.

(64) Smerieri, M.; Vattuone, L.; Costa, D.; Tielens, F.; Savio, L.: Self-Assembly of (S)-Glutamic Acid on Ag(100): A Combined LT-STM and Ab Initio Investigation. *Langmuir* **2010**, *26*, 7208-7215.

(65) Pecharromán, C.; Sobrados, I.; Iglesias, J. E.; González-Carreño, T.; Sanz, J.: Thermal Evolution of Transitional Aluminas Followed by NMR and IR Spectroscopies. *J. Phys. Chem. B* **1999**, *103*, 6160-6170.

(66) Kwak, J. H.; Hu, J.; Lukaski, A.; Kim, D. H.; Szanyi, J.; Peden, C. H. F.: Role of Pentacoordinated Al^{3+} Ions in the High Temperature Phase Transformation of γ–Al_2O_3. *J. Phys. Chem. C* **2008**, *112*, 9486-9492.

(67) Černý, Z.; Macháček, J.; Fusek, J.; Čásenský, B.; Kříž, O.; G. Tuck, D.: Aluminium-27 and ^{71}Ga NMR Studies of the Solution Chemistry of Ga[$AlCl_4$] and Related Compounds. *J. Chem. Soc., Dalton Trans.* **1998**, 1439-1446.

(68) Batista, A. T. F.; Chizallet, C.; Diehl, F.; Taleb, A.-L.; Gay, A.-S.; Ersen, O.; Raybaud, P.: Evaluating Acid and Metallic Site Proximity in Pt/γ–Al_2O_3–Cl Bifunctional Catalysts through an Atomic Scale Geometrical Model. *Nanoscale* **2022**, *14*, 8753-8765.

(69) Kubota, H.; Mine, S.; Toyao, T.; Maeno, Z.; Shimizu, K.: Redox-Driven Reversible Structural Evolution of Isolated Silver Atoms Anchored to Specific Sites on γ–Al_2O_3. *ACS Catal.* **2022**, *12*, 544-559.

FOR TABLE OF CONTENTS ONLY